

**GT2022-84603**

## IMPACTS OF THE ADDITIVE MANUFACTURING PROCESS ON THE ROUGHNESS OF ENGINE SCALE VANES AND COOLING CHANNELS

**Alexander J. Wildgoose and Karen A. Thole**  
Department of Mechanical Engineering  
Pennsylvania State University  
University Park, PA, USA

**Ramesh Subramanian**  
Siemens Energy, Orlando, FL, USA

**Lisa Kersting**  
Siemens Energy, Berlin, Germany

**Anand Kulkarni**  
Siemens Corporation, Charlotte, NC, USA

### ABSTRACT

By leveraging the additive manufacturing platform, development time and costs for turbine component testing can be reduced relative to traditional investment casting. Surface roughness is a key characteristic of the additive manufacturing process that can impact flow, heat transfer, and mechanical integrity of printed components. There are multiple design and build considerations that result in variability in surface roughness especially when additively fabricating complicated three-dimensional vanes and internal cooling passages. This study characterizes the surface roughness of internal cooling passages, vanes, and flat external surface samples made using additive manufacturing, specifically the direct metal laser sintering process. The samples were manufactured with various wall thicknesses, layer thicknesses, build locations, build directions, and on different AM machines. A combination of computed tomography scanning and optical profilometry were used to evaluate surface roughness levels. The data indicates that the dominate factors in roughness for a given layer thickness are a function of wall thickness, build location, and build direction.

### NOMENCLATURE

$A_c$	cross-sectional flow area
$D_h$	hydraulic diameter, $4A_c/p$
LE	leading edge
$p$	channel perimeter
PS	pressure side
$R_a$	arithmetic mean roughness
$R_z$	mean roughness depth
$r$	radial distance from laser source
SS	suction side
$t$	wall thickness
$Z_{max}$	maximum surface height from reference
$Z_{min}$	minimum surface height from reference
$Z_{ref}$	reference surface height
$Z_{surf}$	roughness height

### Greek

$\sigma$	standard deviation
$\Theta$	build direction

### INTRODUCTION

The fabrication guidelines for additive manufacturing (AM), specifically direct metal laser sintering (DMLS) a type of powder bed fusion process, are intrinsically different from traditional subtractive or casting methods. The DMLS process fabricates parts by spreading a layer of metal powder using a recoater blade on top of a build plate (i.e. substrate). A laser then selectively melts the powder particles following the geometry profile of the part. The layer wise process is then repeated until the part is complete. There are multiple considerations that factor into the AM design and fabrication process of a part such as the printability of part features, the layout of the part on the build plate, and the selection of the AM machine. Each sequence in the fabrication of an AM component influences the deviation from design intent of the part [1]. Characterizing the deviation from design intent in terms of surface roughness is important for AM gas turbine parts since roughness impacts the performance and life cycle of the part.

Understanding the major contributions to the roughness for each step of the build sequence, the process from the design of the part to build layout and then machine selection is important in providing reproducible turbine components made through AM. For example, traditionally fabricated nozzle guide vanes typically have highly engineered curved airfoils and experience a range of wall thicknesses that need to be replicated with tight tolerances. The objective of this study was to provide an overview of influences that the AM build sequence has on the part quality of engine relevant internal cooling channels and vane airfoil geometries. Specifically, the roughness for three different geometries were evaluated that included internal cooling channels, nozzle guide vanes, and flat external surface samples.

## LITERATURE REVIEW

The high surface roughness present in additively manufactured parts is a result of the layer wise process leading to the stair stepping effect as well as multiple effects contributing to changes and instabilities of the melt pool [2]. While it is challenging to fully control the melt pool, several process parameters have been identified in the literature that significantly contribute to surface roughness in AM parts such as changes in heat accumulation due part geometry [3,4], laser parameters [5], angle of part surface with respect to build plate [6–8], changes in location on the build plate [9–12], and layer thickness [13–15]. A combination of these parameters is typically seen in the general build sequence of an AM part, starting from the part design to build plate location to machine parameters.

Multiple studies have found that changes to the geometry of a part can influence the deviation from design intent and surface roughness [3,4]. A study from Jamshidinia et al. [3] showed that decreasing the spacing between 1 mm thick walls showed high roughness as result of partial melting of the powder particles from increased heat accumulation. Other literature has focused on the minimal feature size and how that affects roughness. Wu et al. [16] showed a lack of fusion between layers at wall thickness below 0.1 mm for Inconel 718. There is an absence of literature, however, concerning the resulting surface roughness over a range of wall thicknesses that occur in turbine components.

When setting up the build layout of samples, consideration is given to the factors that contribute to deviation from design intent such as build direction. It is well known that downward facing surfaces contain higher surface roughness values compared to upward facing surfaces [6–8]. The past studies that have evaluated surface roughness levels as a function of build direction do so with mostly non-curved surfaces. Complicated curved surfaces such as airfoils have a range of local surface orientations depending on the airfoil build direction. Studies that have additively fabricated airfoils, either vanes or blades [17,18], have primarily focused on structural properties. A study by Krewinkel et al. [18] showed that for the particular build direction of the vane, there was a larger deviation from design intent at the midspan of the pressure side compared to the mid-span of the suction side. However, there were no roughness levels reported.

A few studies have shown that part location on a build plate can influence the as-built surface roughness [9–12]. Laser incidence angle is commonly used to correlate surface roughness dependency on build location. The work from Subramanian et al. [12] and Rott et al. [19] shows that the angle of a surface with respect to the laser source affects the melt pool resulting in increased surface roughness when the part is further from the laser source. The samples used in these studies consist of multi-sided pyramids [9], external surface “chess” pieces [12], and vertically oriented plates [11]. While these studies are thorough in their findings, there is limited knowledge as to whether the same trends are experienced in turbine relevant geometries such as the surfaces of cooling channels and curved surface airfoils.

One of the last build sequence considerations before part removal and heat treatment of an AM part is selecting the appropriate machine and layer thickness. Observations from Subramanian et al. [12] noted that position dependency on roughness followed the same trends for a simple flat surface geometry between single (EOS M290-1) and multi-laser (EOS M400-4) machines. Other machine selection parameters such as layer thickness has been shown to impact the as-built surface roughness and effect material properties [13–15]. A systematic

investigation by Bacchewar et al. [14] showed that for upward facing surfaces, roughness increases as layer thickness increases. The same roughness trend was observed for downward facing surfaces angled between 30° and 90°. It is important to note that the different layer thickness evaluated in this study were created using early generation AM machines that resulted in a high (150 to 190 microns) layer thicknesses relative to the layer thickness used in newer generation AM machines (20 to 80 microns).

The goal of this study is to investigate the impact specific sequences in the AM fabrication process has on the surface roughness of engine scale turbine components. This paper analyzes multiple effects on surface roughness including wall thickness, build direction, build location, different AM machine models, and layer sizes for both internal cooling channels and engine scale vane airfoils.



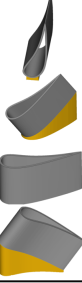

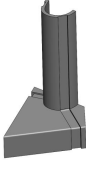
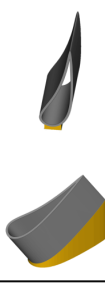
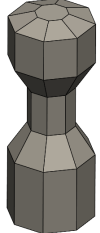

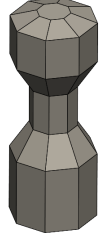
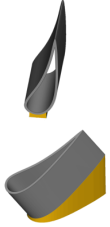
## DESCRIPTION OF SAMPLES

Both internal cooling channels and engine scale vanes were made using AM, specifically DMLS, to evaluate the impact the process and part geometry has on the as-built surface quality of turbine components. As seen by the test matrix in Table 1, the scope of samples used for this study ranged from simple internal cooling channels with a square cross-section to a more complicated engine scale vane to a flat external surface octagonal sample resembling a “chess piece”. The order of samples in Table 1 resembles the additive build sequence. Furthermore, a detailed description of the wall thickness ( $t$ ), radial build location ( $r$ ), build direction ( $\Theta$ ), and machine/layer thickness for each of the samples is shown in Table 1.

To methodically evaluate the impact of the wall thickness, multiple straight channels were placed in a single coupon as shown in Figure 1 and given in Table 1. A 12, 3, 6, and 9 o'clock compass is in Figure 1 that will be used to specify the specific surface orientation in the cooling channel. The distance between the open channel (12 o'clock surface) and the exterior wall was varied between 0.3 mm and 3.0 mm while the bottom of the square channel maintained the same wall thickness as did the spanwise distance between the channels. The channels were equally spaced 4 mm apart from one another to minimize the effect of channel proximity. As seen in Figure 1, the 6 o'clock surface for all the channels was designed with a 2 mm wall thickness to act as a control surface. The particular coupon was placed near the center of the build plate to isolate it from build location effects. The internal channels were fabricated at the 90° (vertical) build direction to limit deformation from the design intent. Build direction is defined as the angle of the surface with respect to the surface of the build plate (i.e. substrate). The internal channel samples in Figure 1 were created using an EOS M280-1 machine (single laser) in Inconel 718 (IN718) with a 40-micron layer thickness using standard EOS recommended process parameters [20]. The samples were solution annealed while attached the build plate using standard EOS IN718 recommended heat treatment parameters [20].

The effects of the wall thickness on more complicated curved surfaces were performed on the leading edge (LE) of a vane as seen in Figure 2 and Table 1. More specifically, the leading edge portion of the National Experimental Turbine (NExT) vane [21]. Similar to the channels, the leading edge vane samples, seen in Figure 2, were fabricated at the 90° build direction where build direction for the vane samples is the angle between the radial axis of the leading edge to the surface of the build plate. The LE vane samples included two different wall

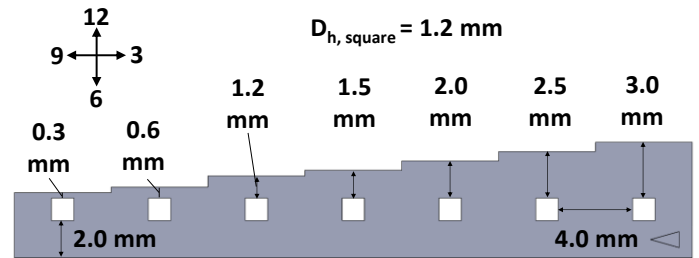
**Table 1. Test Matrix of Internal Cooling, Vane, and “Chess Piece” Samples**

Build Sequence	Part Design		Build Layout				Machine Selection			
Parameter Varied	Wall Thickness		Build Direction	Build Location			Layer Thickness		AM Machines	
t [mm]	0.3 - 3.0	0.4 & 1.4	1.4	2	0.4 & 1.4	1.4	-	1.4	-	1.4
r [mm]	15	75 & 112.5	75	0, 75, 145	75 & 112.5	75, 112.5, 187.5	75	75, 112.5, 187.5	75	75
$\Theta$ [deg]	90°	90°	0°, 60°, 90°, 120°	90°	90°	0° & 60°	-	0° & 60°	-	0° & 60°
Machine & Layer thickness [μm]	280-1 40	M400-1 40	M290-1 40	M280-1 40	M290-1 40	M400-1 40 & 80	M400-1 40 & 80	M400-1 40 & 80	M290-1 40 M400-4 40 M400-1 40	M290-1 40 M400-1 40
Sample Used										

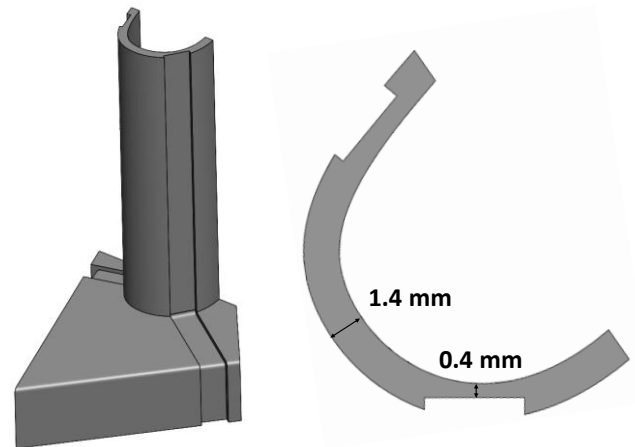
thicknesses (0.4 mm and 1.4 mm) between the interior and exterior of the vane. The largest thickness of the LE vane is at the leading edge nose while the smallest thickness is near the pressure side of the leading edge region as seen in Figure 2. The LE vane samples were manufactured in a 40-micron layer thickness using a single laser EOS M290-1 machine. To investigate build location, the LE vane samples with different wall thicknesses were also manufactured at two different radii (75 mm and 112.5 mm) from the center of the build plate.

Full, hollow NExT vane samples, shown in Figure 3 and highlighted in Table 1, containing no internal or external cooling features were made at different build directions. The NExT vane airfoil samples were fabricated at four orientations (0°, 60°, 90°, 120°) to characterize the variation in surface roughness across the vane. The full vane airfoil samples at different build directions were made using an EOS M290-1 machine with a 40 micron layer thickness. The distinct build orientations in Figure 3 cover a range of airfoil build angles. To minimize the influence of wall thickness on surface roughness, the wall thickness was constant for the full vane samples shown in Figure 3. Furthermore, the vane airfoils at different build directions shared a similar radial location from the laser source in order to reduce the impact of build location on the airfoil surface.

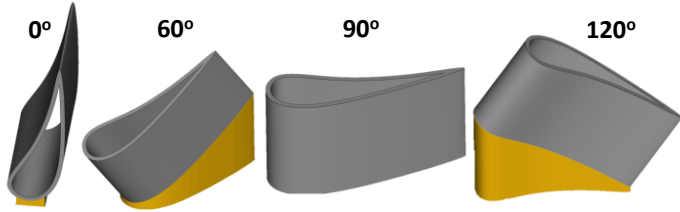
Several of the build directions, specifically the 0° and 60° full NExT vanes were also printed using multiple machines, build locations, and in two different layer thickness as outlined in Table 1. In more detail, a 0° and 60° full vane was printed at three different radii from the laser source ( $r = 75, 112.5, 187.5$  mm) using the EOS M290-1 machine with a 40 micron layer thickness and also a EOS M400-1 machine with 40 and 80 micron layer thicknesses to understand machine differences.



**Figure 1. Schematic of vertically oriented sample with square internal cooling channels at different wall thicknesses fabricated close to the center of the build plate.**



**Figure 2. Leading edge NExT vane [21] samples that were fabricated at three different radii from the laser source and contain two different wall thicknesses between the interior and exterior of the leading edge.**



**Figure 3. NExT vane airfoils without external and internal cooling fabricated across multiple build directions.**

To understand the influence of build location on internal surfaces, several single channel internal cooling samples given in Table 1 and shown in Figure 4, were fabricated at different radial build locations of 0 mm, 75 mm, and 145 mm. The distances of the samples from the laser source were chosen to cover the printable area of an EOS M280 build plate. All internal cooling samples, wall thickness and build location, were designed with a square cross-section channel with a hydraulic diameter of 1.2 mm and a sample height of 14 mm. Each of the samples had a 2 mm wall thickness with a square cross-section. As seen in Figure 4, the single channel samples were fabricated on the same build plate as the channel wall thickness coupon.

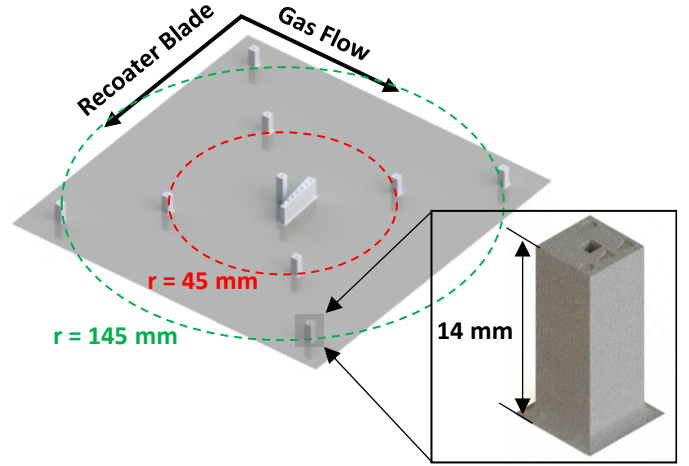
To understand the inherent machine related impact on surface roughness, a standard, symmetrical geometry coupon – “octagonal chess piece” – was printed and is shown in Figure 5. Each coupon has 33 distinct surfaces: one top horizontal, eight 20° upskin, eight 60° upskin, eight 90° vertical, and eight 60° downskin. The coupons alignment in the build plate was identified by a notch oriented towards the gas flow and the letters aligned from left to right, opposite to the recoater direction. As outlined in Table 1, the chess pieces were fabricated using single laser machines (EOS M290-1 and M400-1) and a multi-laser machine (M400-4). The chess pieces were located in each of the print beds at a 75 mm radial location from the laser source. Two layer thickness were investigated – 40 mm and 80 mm (only in M400-1). Siemens Energy proprietary process parameters for IN718 were used in all three machines for the LE vane, full vane, and chess piece samples. A wire electrical discharge machine was used to remove all the samples in Table 1 from their respective build plates. Samples that contained support structures did not have their supports removed.

### INFLUENCE OF WALL THICKNESS ON ROUGHNESS

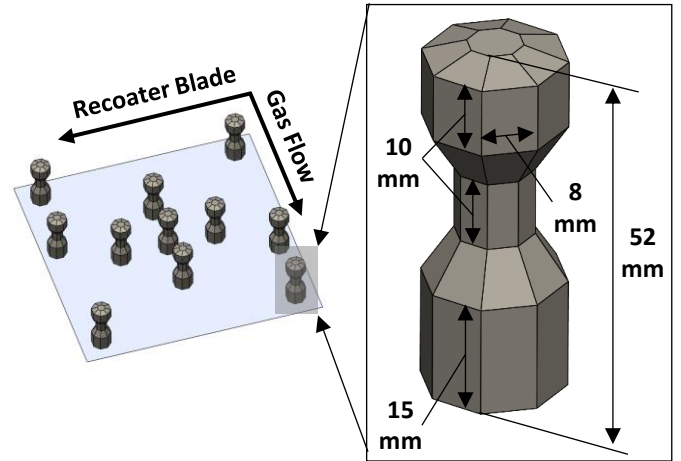
Evaluating the surface roughness of additively manufactured samples gives insight into the as-built quality of the component and the potential enhancement in heat transfer and pressure loss. The surface of the internal cooling channels in Figure 1 were nondestructively evaluated using computed x-ray tomography (CT scans). The surfaces of the channels used for roughness measurements were determined using a commercial software that filters grey scale values obtained from CT scan measurements. The CT scan spatial resolution (i.e. voxel size) of the wall thickness sample shown in Figure 1 was 20 microns. The software is capable of resolving the surface roughness to 1/10<sup>th</sup> of the original voxel size by interpolating the grey scale values [22].

The arithmetic mean roughness, mathematically shown in equation 1, was used to characterize the surface roughness for both the internal cooling and vane samples.

$$R_a = \frac{1}{n} \sum_{i=1}^n |z_{surf} - z_{ref}| \quad (1)$$



**Figure 4. Schematic of vertically oriented internal cooling square channel samples fabricated on an EOS M280-1 at different radii from the center of the single laser source.**



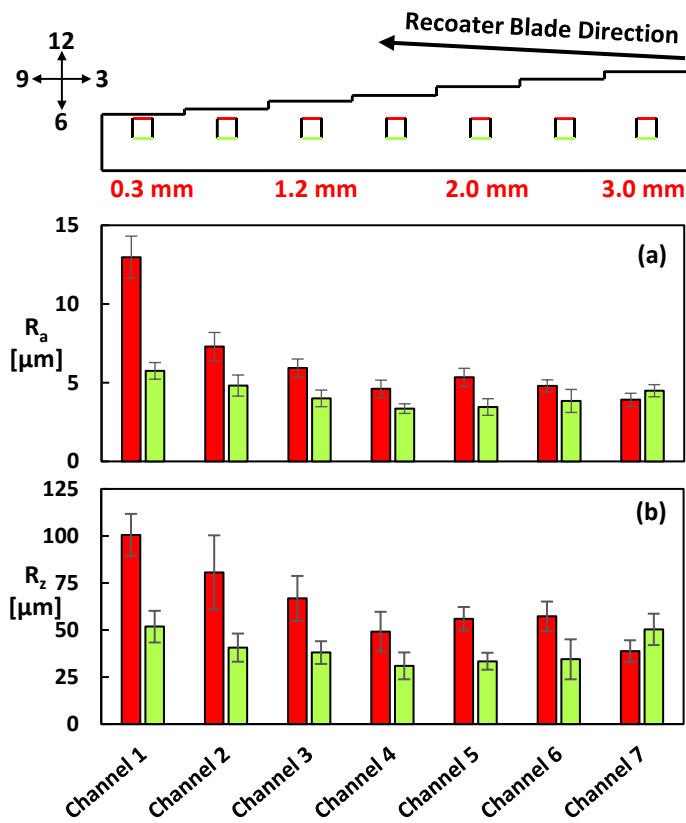
**Figure 5. Build layout of chess piece samples fabricated on different machines using different layer thicknesses.**

The arithmetic mean roughness describes the average deviation of a surface from a reference value. As such, the surface roughness calculated using CT scans was measured by recording the average deviation from the surface relative to a 0.8 mm by 0.8 mm gaussian fitted reference plane. The calculation of arithmetic mean roughness matches the definition for the area averaged arithmetic mean roughness,  $R_a$ . A minimum of five reference planes were fitted to each surface orientation of a cooling channel. The  $R_a$  values of a particular surface orientation (i.e. 6 o'clock) is averaged from using the five planes.

The same five reference planes were also used to calculate the mean roughness depth for the variable wall thickness sample shown in Figure 1. The mean roughness depth, mathematically shown in equation 2, describes the average difference between the highest and lowest points for the five planes.

$$R_z = \frac{1}{5} \sum_{i=1}^5 (z_{max} - z_{min})_i \quad (2)$$

Both surface roughness values calculated for each of the channel wall thicknesses shown in Figure 1 are reported in Figure 6. These results indicate that as wall thickness decreases the

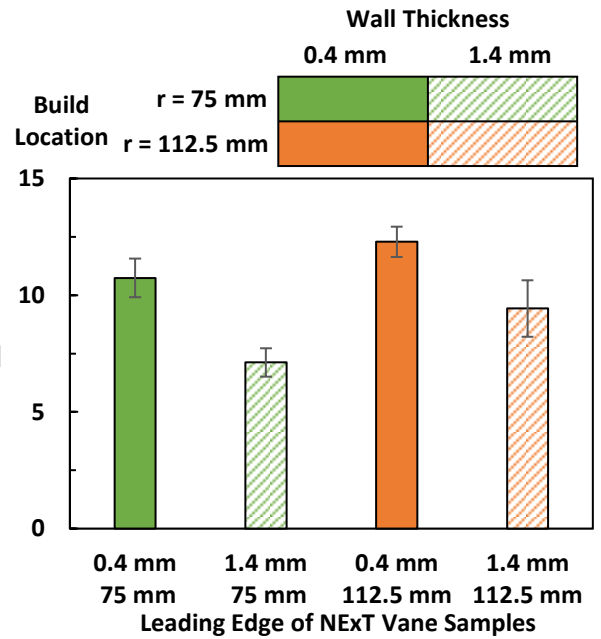


**Figure 6. Arithmetic mean roughness (6a) and mean roughness depth (6b) of internal wall thickness sample measured from CT scan data of the 6 and 12 o'clock surface orientations.**

arithmetic mean roughness gradually increases. The roughness measurements for a particular surface in Figure 6 are accompanied by their 95% confidence interval along with each surface roughness measurement being color matched to the specific surface orientation.

As seen for the 12 o'clock surface in Figure 6(a) by changing the wall thickness of a geometry from 3 mm to 0.3 mm, the arithmetic mean roughness increases 231%. In comparison, the 6 o'clock control surface contained a relatively constant surface roughness with a maximum roughness difference of 25% as a result of the constant 2 mm wall thickness. It would be expected that the roughness levels would be similar for the channels in Figure 1 since they were all built vertically. However, a higher 12 o'clock surface roughness is observed for the thinner wall channels relative to the channels with thicker walls. The cause for the roughness differences is a result of a higher conduction resistance for the thinner wall channels compared to the thicker wall channels impacting the heat accumulation causing a disruption to the melt pool leading to more partially melted particles adhering to the solidified surfaces [3]. While the arithmetic mean roughness gradually increases with wall thickness, the increase in surface roughness only begins to become substantial at a thickness below 0.6 mm.

The mean roughness depth,  $R_z$ , for the variable wall thickness sample, Figure 6(b), follows similar trends to the arithmetic mean roughness where roughness increases as wall thickness decreases. More specifically, there is a 160% increase in mean roughness depth when changing wall thickness from 3 mm to 0.3 mm. Similar to the arithmetic mean roughness, the 6 o'clock control surface contained a relatively constant mean roughness depth with a maximum roughness difference of 50%.



**Figure 7. Arithmetic mean roughness measured using CT scan data of the different wall thickness and build location leading edge NExT vanes samples fabricated on the EOS M290-1 in a 40 micron layer thickness, seen in Figure 2.**

Also important to note from Figure 6 is that there can be a significant difference in arithmetic mean surface roughness for two different walls in a given channel. For example, in channel 1 there is a 77% difference between the 12 o'clock (0.3 mm) and 6 o'clock (3 mm) channel. The amount of variation in surface roughness caused by wall thickness will have a substantial impact to the local convective heat transfer.

The influence of wall thickness on surface roughness for more complicated geometries such as the curved vane leading edge illustrated in Figure 2 was also investigated using CT scanning. The same procedure and voxel size for calculating the surface roughness of the internal cooling channel wall thickness sample was used for the roughness measurements of the LE vane samples. More specifically, the same square Gaussian fitted planes as the internal cooling channels were applied along the radial direction of the vane samples in Figure 2.

Similar to the results for the channels, the surface roughness increases with decreasing wall thickness for both of the LE vane samples as seen in Figure 7. The surface roughness is 51% higher at a wall thickness of 0.4 mm compared to a wall thickness of 1.4 mm for the coupon closest to the laser source. The surface roughness is 30% higher at a wall thickness of 0.4 mm compared to a wall thickness of 1.4 mm for the vane coupon furthest from the laser source. Even though the samples were fabricated at two different build locations, the arithmetic mean roughness measurements show that both samples contain higher roughness levels for the thinner walls.

Investment cast vanes traditionally used in turbines also contain a wide range of wall thickness both between the cooling passages themselves as well as thicknesses of the airfoil. The results from Figures 6 and 7 suggest that wall thickness can directly impact the as-built surface roughness regardless of surface curvature. These results imply that the surfaces near the trailing edge of a vane, where wall thickness is typically very thin, are expected to have a higher surface roughness compared to other regions of a vane when using AM.



## EFFECT OF BUILD DIRECTION ON VANE ROUGHNESS

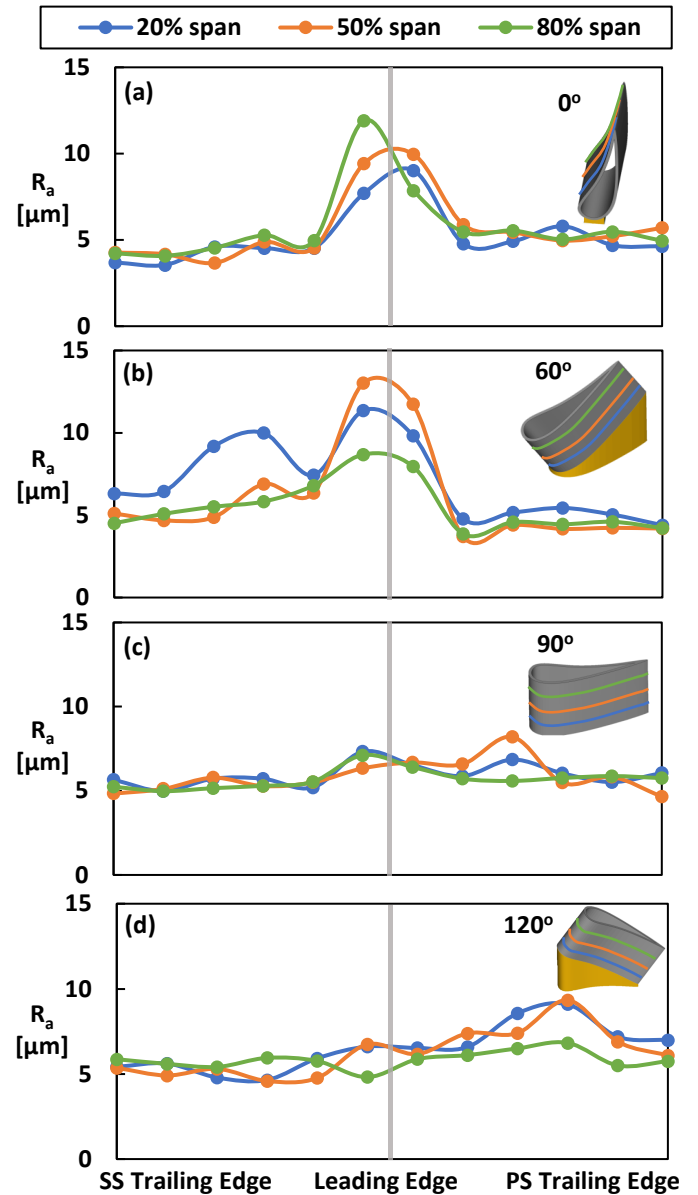
The surface roughness, given by equation 1, of multiple engine scale vane airfoils printed at multiple build directions was characterized using optical profilometry (OP) to understand the variation in roughness along the length of the curved surfaces of the NExT vanes. Having a direct line of sight to the surface provided the possibility of OP measurements to evaluate the external surface of the vanes in Figure 3. OP measurements capture more detail of the surface relative to CT scan measurements because of the higher measurement resolution. When comparing CT scan to OP measurements, Snyder et al. [23] observed that CT measurements show similar trends as OP measurements despite reduced  $R_a$  values using the CT scans. More specifically, CT scans are equivalent to applying a low pass filter to the surface, thus being able to resolve the larger roughness features such as dross compared to the smaller partially melted particles that the OP method is able to resolve.

Multiple 0.8 mm by 0.8 mm sample sizes using OP were taken at 20% span, 50% span, and 80% span of both the suction, leading edge, and pressure side of the NExT vanes. More specifically, the OP measurements were performed using Sensofar S-Neox90, with the focus variation setup. In this measurement mode, an entire Z-range that extends from the lowest valley to the highest peak is scanned. From the scanned images, a 3D image composed of stacked images was compiled and a 3D image was reconstructed. Images were taken with an objective lens 10X and the surface roughness measurement requirements of 0.8 mm cut-off length, with a L-Gaussian correction was evaluated to meet ISO 4287 standards, after application of a 5x5 median denoising filter.

The  $R_a$  values for the NExT vanes shown in Figure 8 indicate that build direction results in as much as a 300% difference depending upon locations on the same vane. The curvature of a vane can result in the local surface containing a range of angles with respect to the build plate. Similar to external and internal surface literature [6,8,24,25], surfaces that are downward facing contain higher roughness levels relative to upward facing surfaces. As the vane orientation increases from 0° to 120°, the roughness of both the leading edge, suction side, and pressure side changes according to the local surface angle with respect to the build plate.

The leading edge portion of the 0° vane in Figure 8(a) contains a significantly higher surface roughness compared to the suction side and pressure side of the vane as a result of the downward facing leading edge surface. While not immediately noticeable, the surface roughness of the 0° vane trailing edge suction side is 19% lower compared to the trailing edge pressure side. The cause for the roughness difference is because the surfaces of the suction side trailing edge gradually become upward facing compared to the downward facing surfaces of the pressure side trailing edge due to the curvature of the vane. When comparing the 0° vane to the other orientations in Figure 8, the 0° vane has the highest roughness on the leading edge nose. There is minimal difference in roughness on the 0° vane at different span wise locations.

In contrast, the 60° vane in Figure 8(b) contains a wide range of roughness levels at different spanwise locations on the suction side and leading edge nose. Surface roughness of the 60° vane is the most non-uniform compared to all other build directions. Surface roughness for the 60° vane is highest at the leading edge nose followed by the suction side then pressure side. The cause for the nonuniformity in surface roughness of the 60°



**Figure 8. Arithmetic mean roughness measured using an optical profilometer across the pressure side, suction side, and leading edge NExT vane airfoils printed at 0° (8a), 60° (8b), 90° (8c), and 120° (8d) on an EOS M290-1 at a 40 micron layer thickness.**

vane is a result of the change in laser incidence angle along the suction side part surface.

Roughness is lowest and most uniform across the airfoil when the leading edge of a vane is parallel to the build direction as seen in Figure 8(c). The 90° airfoil contains the lowest surface roughness across the range of build directions evaluated due to the airfoil containing no downward facing surfaces. Since both the external and internal surfaces of the vane share the same 90° build direction, it is speculated that the surface roughness of the interior portion is similar in uniformity as the measured external airfoil surface. The results from Figure 8(c) infer that when all the curved surfaces share the same build direction in this case 90°, the differences in surface roughness are minimal; however, for the build directions other than 90°, the interior surface of the airfoils are different from the exterior. For example, the leading edge external surface roughness of the 60° vane is highest relative

to other external locations. While the interior portion of the leading edge 60° vane was not measured, the surface is upward facing which will most likely result in a lower roughness relative to the downward facing external surface of the leading edge airfoil. The exterior surfaces of the vanes in Figure 8 that are upward facing contain interior surfaces that are downfacing.

By orienting the leading edge of a vane to 120° from the build plate, surface roughness increases from the leading edge to the trailing edge of the pressure side and varies little across the spanwise locations as in Figure 8(d). The cause for the increase in roughness is attributed to the curvature of the airfoil, more specifically the downward facing surfaces of the pressure side relative to the upward facing surfaces of the leading edge nose and the area near the leading edge of the suction side. The roughness distribution across the airfoils between the 0°, 60°, and 120° samples emphasizes the importance of the local surface angle of a curved surface.

Even though the 90° build for the vane is the most optimal in terms of the lowest external roughness, it is important to note that no cooling features were present in the sample for the data in Figure 8. A full additively made vane at the 90° leading edge build direction would most likely require trailing edge cooling passages needing a geometry correction since the cooling passages would be fabricated parallel to the build plate. Furthermore, multiple external supports would be needed to minimize deformation of the fir tree since these features have a high possibility of being built parallel to the build plate when the leading edge is at 90°.

By orienting the vane to 0°, 60°, or 120°, internal passages at the trailing edge are most likely to contain less severe downward facing surfaces and require less geometric corrections relative to the 90° vane. Designers must also consider the orientation of cooling passages at the leading edge and mid region of vanes. A combination of geometry and local surface orientations need to be considered for desired external and internal surface roughness when orienting a curved component.

### IMPACT OF BUILD LOCATION ON ROUGHNESS

The roughness values of the internal cooling channel samples at different build locations in Figure 4 were analyzed using the same CT scan roughness procedure outlined for the internal channel wall thickness sample. The voxel resolution for the internal cooling channels at different build directions was lower, 15 microns, compared to the channel wall thickness sample because of a smaller scan area. Contours of  $R_a$ , calculated using equation 1, changing with build location is shown in Figure 9. The roughness contour is linearly interpolated between the average surface roughness from all surfaces in each of the square internal channels at different build locations. More specifically, the roughness for each sample is averaged using five 0.8 mm by 0.8 mm planes fitted to each side of the square cooling channels.

Similar to external flat surface literature [11,12,19], build location has a considerable impact on the surface roughness for internal surfaces as seen in Figure 9 and Figure 10. As components are built further from the laser source (i.e. center of build plate for EOS M280-1) the surface roughness increases. Quantitatively, there is a 10% increase in roughness from the center of the build plate to a radial distance of 75 mm. While the roughness is 35% higher from the build plate center to a radial distance of 145 mm. The change in laser incidence angle relative to the part surface causes the melt pool dynamics to change depending on build location resulting in the as-built surface

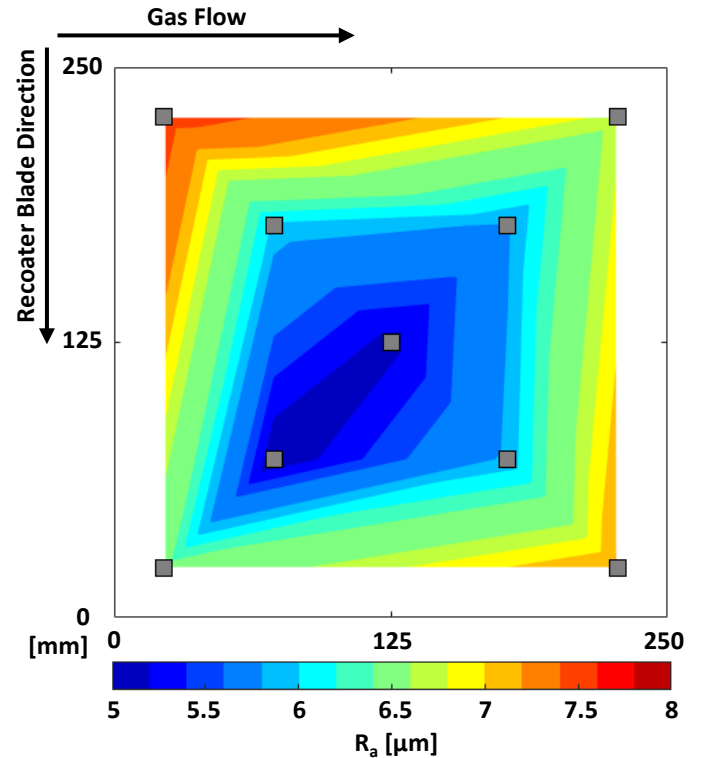


Figure 9. Build plate contour of average arithmetic mean roughness measured using CT scan data from the four internal surfaces of the square cooling channel.

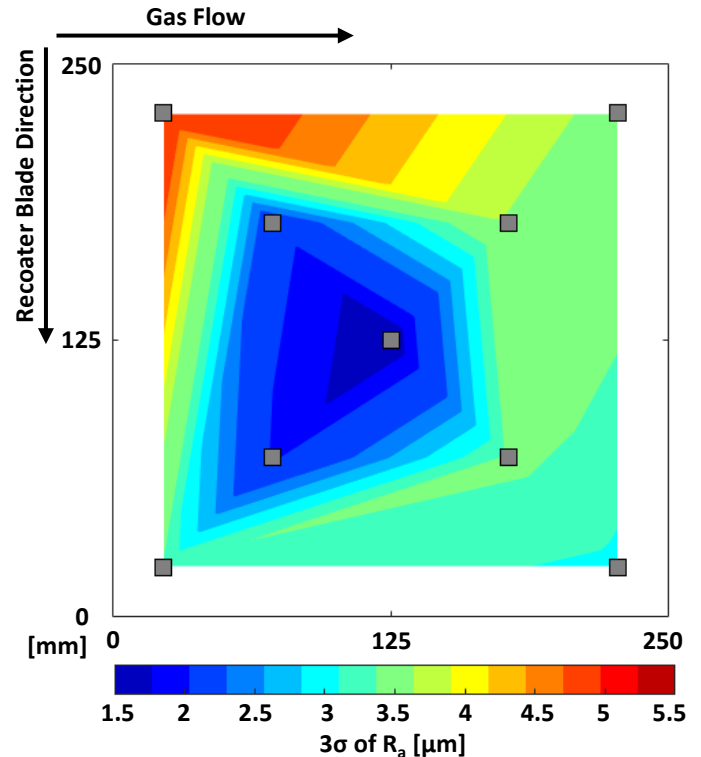


Figure 10. Build plate contour of the 3 $\sigma$  deviation of arithmetic mean roughness measured using CT scan data from the four internal surfaces of the square cooling channel.

roughness to increase the further the part is from the laser source [9,12]. The results from Figure 9 show that it is possible for the surface roughness to become nonuniform for very large parts because of the change in laser incidence angle along the length of

the part. The increase in roughness is observed regardless of the proximity the channel is to the origin of the gas flow and beginning of the recoater blade process. With the addition of more samples on the build plate in Figure 9, the as-built surface roughness from a particular machine can be recorded.

The variation in surface roughness also increases the further a part is from the laser source as seen by the standard deviation contour of arithmetic mean roughness in Figure 10. On average there is a 79% increase in the  $3\sigma$  deviation when an internal surface is at the center of the build plate to when the surface is at radial distance of 75 mm from the center. Whereas there is a 142% increase from the center of the build plate to a radial distance of 145 mm. The implications of these results are that internal surfaces are lower in roughness and are more reproducible the closer the part is to the laser source.

The LE vane samples in Figure 7 share the same roughness trends of the internal cooling channels in Figure 9, where the roughness increases the further the part is from the laser source. It is important to acknowledge that the roughness trends match even though the LE vane and channel samples were built on separate EOS machine models and the geometries of the parts are different. When comparing the two LE vane samples with different wall thickness in Figure 7, there is a 14% increase in roughness between the LE vane sample at a radial distance of 75 mm relative to 112.5 mm for the 0.4 wall thickness. Similarly, there is a 32% increase in roughness for the 1.4 mm wall thickness region between 75 mm to 112.5 mm sample location.

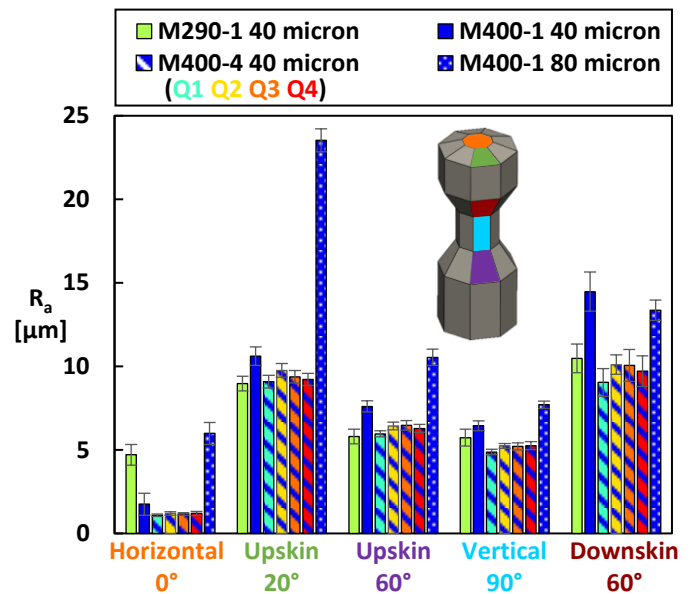
Recall that for a given build location of the LE vane samples, surface roughness was still influenced by wall thickness. These results suggest that a combination of wall thickness and changes in build location contributed to the differences in as-built surface roughness of the LE vane samples. For cooling applications using AM, the results from Figure 7 and Figure 9 show that surface roughness of a component can be altered by changing the build location. The added roughness from moving a part further from the laser source can most likely increase the convective heat transfer with the cost of additional pressure loss for cooling channels. Additionally, the surface of the part will become less uniform the further it is from the laser source.

## EFFECT OF LAYER THICKNESS AND MACHINE TYPE

The surface roughness,  $R_a$ , at multiple surface orientations of the chess piece in Table 1 are given by Figure 11 using the OP method. Each chess piece that was fabricated at each of the four quadrants (Q1, Q2, Q3, Q4) in the four laser M400-4 are colored coded in Figure 11. Each surface roughness bar in Figure 11 represents the average roughness of over 80 roughness measurements. In more detail, 11 OP measurements were made for each side (total of eight) of the chess piece sample. The error bars in Figure 11 represents the 95% confidence interval of the averaged roughness data.

Results from Figure 11 indicate that there is a minimal difference (less than 1 micron) in surface roughness at every surface orientation for the four samples printed using the different lasers in the M400-4 machine. It is important to note that the samples printed at each of the four queens in the M400-4 shared the same radial distance from the laser source.

Similar to layer thickness trends in literature [14], the surface roughness is greater at a 80 micron layer thickness relative to a 40 micron layer thickness as seen in the external surfaces of the chess piece samples in Figure 11. On average, the arithmetic mean roughness for the 80 micron layer thickness is 1



**Figure 11. Average of 88 arithmetic mean roughness values for each surface of the “chess piece” fabricated using two different single laser machines, two layer thickness, and a four laser machine.**

to 13 microns higher compared to the 40 micron layer thickness for all surface orientations, except the downskin 60°, of the chess piece created using the M400-1 machine.

For all the surface orientations evaluated across the chess piece samples that were made using the different machines, surface roughness was typically the highest on the 60° downskin followed by the 20° upskin, 60° upskin, 90° vertical, then 0° horizontal surface orientations. The only machine that did not follow this trend was the M400-1 for an 80 micron layer thickness. The surface roughness of the M400-1 80 micron layer thickness is higher for the 20° upskin surface compared to the 60° downskin surface. After further investigation, the cause is a result of the stair stepping effect, which was exacerbated due to the 80 micron layer thickness relative to a 40 micron layer thickness, that led to an increase in roughness for the 20° upskin surface compared to the 60° downskin surface.

It is clear from the results in Figure 11, that the surface roughness across all three machines (M290-1, M400-1, M400-4) for a 40 micron layer thickness are very similar with less than a 5 micron difference. Some surface orientations such as the upskin 20°, upskin 60°, and vertical 90° are less than a 2 micron difference between the 40 micron layer thickness machines. The small difference in roughness level highlights that the machine induced surface roughness variation is minimal on flat surfaces. In comparing the roughness of the single laser machines at a 40 micron layer thickness (M290-1 and M400-1), the roughness is 16-28% lower for the M290-1 compared to the M400-1 for all surface orientations except for the horizontal 0° surface orientation. The surface roughness values across all build orientations were 13-51% higher for the single laser M400-1 chess piece sample compared to the four samples created at the different quadrants using the multi-laser M400-4.

The surface roughness was also evaluated for the 0° and 60° full NExT vane created using different AM machines (M400-1 and M290-1), different radial build locations (75 mm, 112.5 mm, 187.5), and different layer thickness (40 micron for the M290-1 and 40/80 micron for the M400-1). The mid-span OP



measurements in Figure 12 followed the same measurement method as the vanes in Figure 8. The roughness trends from the pressure side to suction side of the airfoil for the 0° and 60° vanes in Figure 12 are mostly similar regardless of machine used. Near the leading edge nose for the 0° and 60° vane the surface roughness is highest due to the surface being downfacing compared to the surfaces of the suction side and pressure side. Furthermore, the surface roughness differences between the leading edge and suction and pressure side are due to the complex angles of the laser to the surface and the local scan pattern adjustments done to accommodate for the local curvature. This effect would require more detail to understand the role of extreme curvature on surface roughness values.

Similar to the internal channel roughness results in Figure 9 and the LE vane samples in Figure 7, the surface roughness for a vane increases the further it is built from the laser source regardless of build direction and layer thickness as seen in Figure 12. These results further support that the distance from the surface to the laser source is a major influence to roughness.

Similar to the flat surface chess piece samples, the surface roughness for the 60° vane with an 80 micron layer is higher compared to its 40 micron equivalent using the M400-1. However, the peak roughness value for the 80 micron layer thickness is near the leading edge pressure side while the peak roughness value for the 40 micron process is near the leading edge suction side. The cause for the discrepancy could be a result of the differences in layer thickness causing a more prominent stair stepping effect to occur. When comparing layer thicknesses for the 0° vane in Figure 12(a), the surface roughness is lower for the 80 micron process compared to the 40 micron process of the M400-1. Again, the cause for the result is the difference in layer thickness impacting the stair stepping effect for the specific surface orientation as well as differences in process parameters used for the two layer thicknesses.

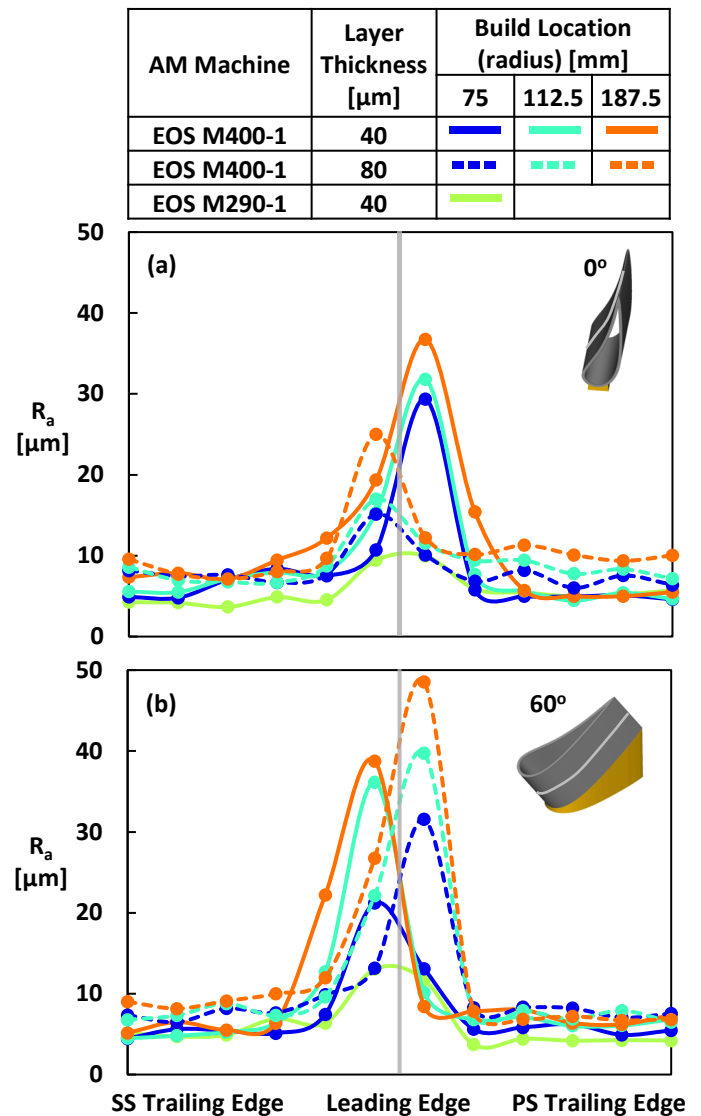
Matching the same roughness trend for the M400-1 and M290-1 flat chess pieces surfaces in Figure 11, the surface roughness for the 0° and 60° vanes with a 40 micron layer thickness printed at different build locations is higher for the M400-1 compared to the M290-1. For the build plates of the vanes and chess pieces, surface roughness appears to be higher using the M290-1 compared to the M400-1.

## CONCLUSION

Multiple engine relevant samples were fabricated using DMLS to investigate the influence the additive build sequence, spanning part design, build layout and machine selection, has on the as-built surface quality of engine scale vanes, cooling channels, and simple external surface samples. Specifically, the samples were fabricated with a variety of wall thicknesses, build directions, build locations, layer thicknesses, and different AM machines. CT scanning and optical profilometry was used to measure surface roughness in order to characterize the as-built surface quality of the vane and cooling channel samples.

Roughness results from vanes and cooling channels with varying wall thickness, show that that changes to the geometry of a component, specifically the wall thickness, can impact the surface roughness. As wall thickness decreases the surface roughness increases for both vanes and simple square cross-section channels. The surface roughness of the channels begins to substantially increase at wall thicknesses below 0.6 mm.

The full airfoil of the NExT vane was fabricated across four distinct build directions. The surface roughness was uniform



**Figure 12. Arithmetic mean roughness Arithmetic using an optical profilometer across the pressure side, suction side, and leading edge of the NExT vane airfoils fabricated at the 0° (12a) and 60° (12b) build direction using different AM machines, build locations, and layer thicknesses.**

across the spanwise locations for the vanes fabricated with the leading edge at the angle of 0°, 90°, and 120° from the build plate. For several build directions, the curvature of the airfoils resulted in varying levels of surface roughness across the pressure side, suction side, and leading edge of the airfoil. Designers additively fabricating vanes should consider the local surface orientations on the airfoils and the build directions of the internal passages.

The location of samples on the build plate has a direct influence on surface roughness. Both cooling channels, the leading edge portion of the NExT vane, and full NExT vane airfoil were fabricated at different radii from the laser source. For both sets of samples, the surface roughness increases the further the sample is from the laser source. Even with some samples containing changes to wall thickness and build direction, the trend of increasing roughness with increasing distance from the laser source was observed.

Several test samples with external surface resembling a “chess piece” and a full vane at two different build directions were fabricated on different EOS machines using two different

layer thickness (40 and 80 microns) along with single and multi-laser setups. Surface roughness was higher in the 80 micron layer thickness relative to the 40 micron layer thickness for most surface orientations of the vanes and the chess piece samples. There were minimal variations in surface roughness between samples fabricated at different quadrants of a four laser EOS M400-4 machine. Roughness for multiple samples was higher for a M400-1 relative to a M290-1 in a 40 micron layer thickness.

Findings from these AM studies and those in the future will continue to advance metal AM to produce repeatable complicated geometries. Understanding the major factors that affect surface roughness for each build sequence in the general AM process is important for the reproducibility and fabrication of vanes and cooling channels. The results from this study indicate that the major influences on surface roughness for flat and curved surface samples at a given layer thickness are build location, build direction, and wall thickness.

## ACKNOWLEDGMENT

The authors would like to acknowledge the funding provided by the U.S. Department of Energy National Energy Technology Laboratory. At Penn State, we would like to recognize the efforts in fabricating the coupons with Corey Dickman and members at Penn State's CIMP-3D lab. The authors thank Timothy Stecko and Whitney Yetter for performing the CT scans. At Siemens Energy, we would like to thank Michael Pepperman for systematic efforts in surface roughness measurements. We would also like to thank John Rapp and Ross Henrys for printing the coupons.

## REFERENCES

- [1] Rehme, O., 2010, *Cellular Design for Laser Freeform Fabrication*, Cuvillier Verlag.
- [2] Sendino, S., Martinez, S., Lamikiz, A., Lartategui, F., Gardon, M., and Gonzalez, J. J., "Analytical Study of the Melt Pool Distortion in the Laser Powder Bed Fusion Process Caused by the Angle of Incidence of the Laser and Its Effect on the Surface Finish of the Part."
- [3] Jamshidinia, M., and Kovacevic, R., 2015, "The Influence of Heat Accumulation on the Surface Roughness in Powder-Bed Additive Manufacturing," *Surf. Topogr. Metrol. Prop.*, **3**(1), p. 014003.
- [4] Yeung, H., Lane, B., and Fox, J., 2019, "Part Geometry and Conduction-Based Laser Power Control for Powder Bed Fusion Additive Manufacturing," *Addit. Manuf.*, **30**, p. 100844.
- [5] Snyder, J. C., and Thole, K. A., 2020, "Tailoring Surface Roughness Using Additive Manufacturing to Improve Internal Cooling," *J. Turbomach.*, **142**(7), pp. 1–12.
- [6] Ventola, L., Robotti, F., Dialameh, M., Calignano, F., Manfredi, D., Chiavazzo, E., and Asinari, P., 2014, "Rough Surfaces with Enhanced Heat Transfer for Electronics Cooling by Direct Metal Laser Sintering," *Int. J. Heat Mass Transf.*, **75**, pp. 58–74.
- [7] Tian, Y., Tomus, D., Rometsch, P., and Wu, X., 2016, "Influences of Processing Parameters on Surface Roughness of Hastelloy X Produced by Selective Laser Melting," *Addit. Manuf.*, **13**, pp. 103–112.
- [8] Pakkanen, J., Calignano, F., Trevisan, F., Lorusso, M., Ambrosio, E. P., Manfredi, D., and Fino, P., 2016, "Study of Internal Channel Surface Roughnesses Manufactured by Selective Laser Melting in Aluminum and Titanium Alloys," *Metall. Mater. Trans. A Phys. Metall. Mater. Sci.*, **47**(8), pp. 3837–3844.
- [9] Kleszczynski, S., Ladewig, A., Friedberger, K., Jacobsmuhlen, J. zur, Merhof, D., and G, W., 2015, "Position Dependency of Surface Roughness in Parts From Laser Beam," *SFF Symp. Proc.*, pp. 360–370.
- [10] Oter, Z. C., Coskun, M., Akca, Y., Surmen, O., Yilmaz, M. S., Ozer, G., Tarakci, G., Khan, H. M., and Koc, E., 2019, "Support Optimization for Overhanging Parts in Direct Metal Laser Sintering," *Optik (Stuttg.)*, **181**, pp. 575–581.
- [11] Sendino, S., Gardon, M., Lartategui, F., Martinez, S., and Lamikiz, A., 2020, "The Effect of the Laser Incidence Angle in the Surface of L-Pbf Processed Parts," *Coatings*, **10**(11), pp. 1–12.
- [12] Subramanian, R., Rule, D., and Nazik, O., 2021, "Dependence of LPBF Surface Roughness on Laser Incidence Angle and Component Build Orientation," *Proceedings of the ASME Turbo Expo GT2021-597*.
- [13] Strano, G., Hao, L., Everson, R. M., and Evans, K. E., 2013, "Surface Roughness Analysis, Modelling and Prediction in Selective Laser Melting," *J. Mater. Process. Technol.*, **213**(4), pp. 589–597.
- [14] Bacchewar, P. B., Singhal, S. K., and Pandey, P. M., "Statistical Modelling and Optimization of Surface Roughness in the Selective Laser Sintering Process."
- [15] Wegner, A., and Witt, G., 2012, "Correlation of Process Parameters and Part Properties in Laser Sintering Using Response Surface Modeling," *Physics Procedia*, pp. 480–490.
- [16] Wu, Z., Narra, S. P., and Rollett, A., 2020, "Exploring the Fabrication Limits of Thin-Wall Structures in a Laser Powder Bed Fusion Process," *Int. J. Adv. Manuf. Technol.*, **110**(1–2), pp. 191–207.
- [17] Kaplanskii, Y. Y., Levashov, E. A., Korotitskiy, A. V., Loginov, P. A., Sentyurina, Z. A., and Mazalov, A. B., 2020, "Influence of Aging and HIP Treatment on the Structure and Properties of NiAl-Based Turbine Blades Manufactured by Laser Powder Bed Fusion," *Addit. Manuf.*, **31**.
- [18] Krewinkel, R., Such, A., de la Torre, A. O., Wiedermann, A., Castillo, D., Rodriguez, S. A., Schleifenbaum, J. H., and Blaswich, M., 2020, "Design and Characterization of Additively Manufactured NGVs Operated in a Small Industrial Gas Turbine," *Int. J. Gas Turbine, Propuls. Power Syst.*, **11**(4).
- [19] Rott, S., Ladewig, A., Friedberger, K., Casper, J., Full, M., and Schleifenbaum, J. H., 2020, "Surface Roughness in Laser Powder Bed Fusion – Interdependency of Surface Orientation and Laser Incidence," *Addit. Manuf.*, **36**, p. 101437.
- [20] EOS, 2011, *Basic Training EOSINT M280*, Electro Optical Systems GmbH, Munich, Germany.
- [21] Thole, K. A., Barringer, M., Berdanier, R. A., Fishbone, S., Wagner, J., Dennis, R., Black, J., Burke, P., Straub, D., O'Neill, F., Stimpson, C., Riahi, A., Aggarwala, A., Bradshaw, S., Kohli, A., Mongillo, D., Praisner, T., Rodriguez, J., Fox, M., and Kim, Y., 2021, "Defining a Testbed for the U.S. Turbine Industry: The National Experimental Turbine (NEXt)," American Institute of Aeronautics and Astronautics (AIAA).
- [22] Reinhart, C., 2011, *Industrial CT & Precision*, Volume

Graphics GmbH, Heidelberg, Germany.

- [23] Snyder, J. C., and Thole, K. A., 2020, “Understanding Laser Powder Bed Fusion Surface Roughness,” *J. Manuf. Sci. Eng. Trans. ASME*, **142**(7).
- [24] Wildgoose, A. J., Thole, K. A., Sanders, P., and Wang, L., 2021, “Impact of Additive Manufacturing on Internal Cooling Channels with Varying Diameters and Build Directions,” *J. Turbomach.*, **143**(7), p. 071003.
- [25] Stimpson, C. K., Snyder, J. C., Thole, K. A., and Mongillo, D., 2017, “Scaling Roughness Effects on Pressure Loss and Heat Transfer of Additively Manufactured Channels,” *J. Turbomach.*, **139**(2), p. 021003.